On the need for high Reynolds number wind tunnel facilities for environmental turbulence research.

Zellman Warhaft and Lance Collins. Cornell

- With :Sathyanarayana Ayyalasomayajula, Cornell University.
- Armann Gylfason, Reykjavik
- Eberhard Bodenshatz,Goettingen & Cornell
- Raymond Shaw , Michigan Technical University

- Thanks to H. Xu, N. Ouellette,H.Nobach(Cornell-Max Planck),
- Todd Cowen(Cornell)
- and E.W.Saw, P. Y . Chuang (MTU)
- NSF

Turbulence in Clouds

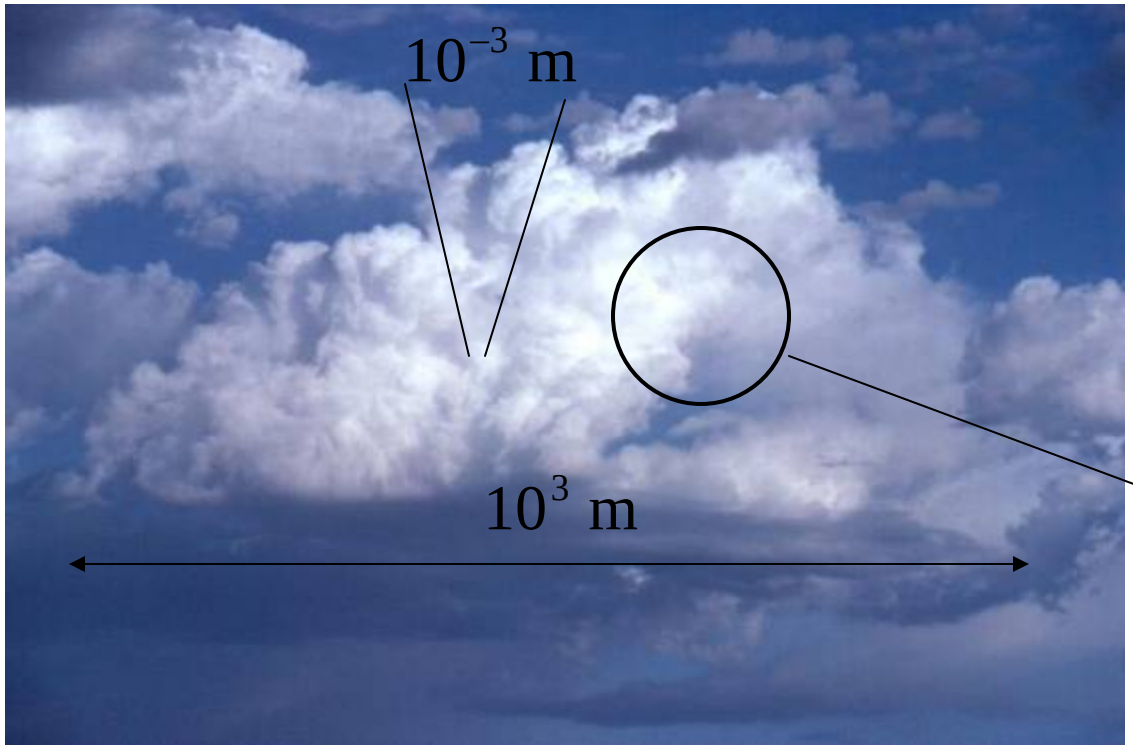

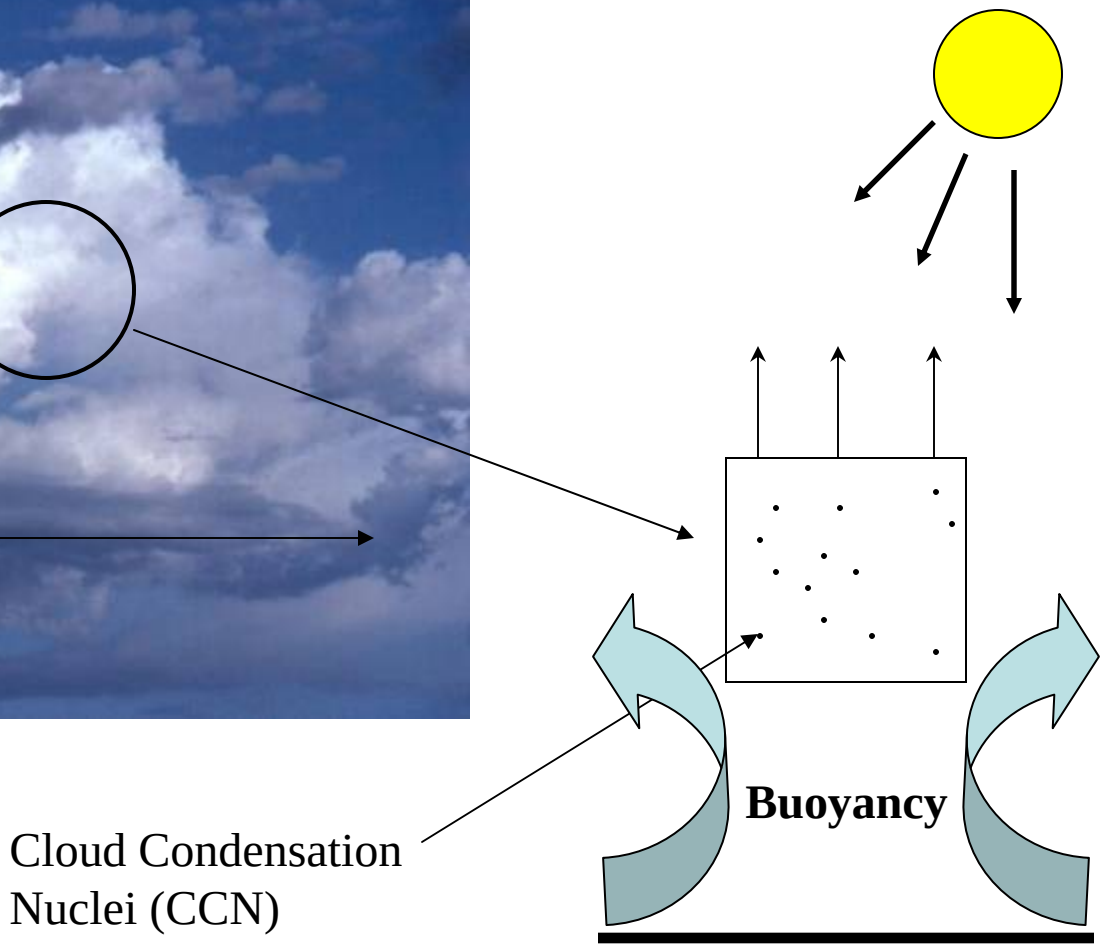

Clustering of inertial particles

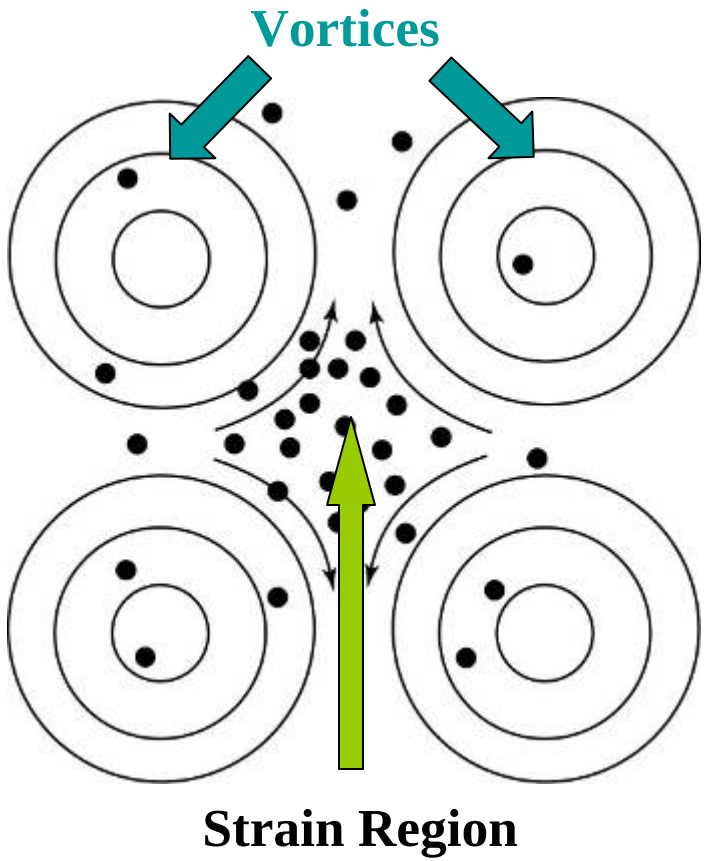

- Maxey (1987); Squires & Eaton (1991); Wang & Maxey (1993)
- Shaw, Reade, Verlinde & Collins (1997)
- Falkovich, Fouxon & Stepanov (2002); Zaichik & Alipchenkov (2003); Chun, Koch, Rani, Ahluwalia & Collins (2005)

TOPICS

--Inertial and fluid particles : Lagrangian measurements

--The Lagrangian pdf and its dependence on Reynolds and Stokes number

--The radial distribution function

--Pair dispersion

--Anisotropy at high Reynolds number

--Impact on environmental flows

Typical Run

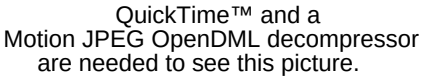
QuickTime™ and a
Motion JPEG OpenDML decompressor
are needed to see this picture.

Experimental Specifications

Makita active grid

- $R_\lambda = 253$
- $\tau_\eta = 12.7$ msec
- $\varepsilon = 0.093\ m^2/sec^3$
- $\nu = 1.5 \times 10^{-5}\ m^2/sec$

QuickTime™ and a
YUV420 codec decompressor
are needed to see this picture.

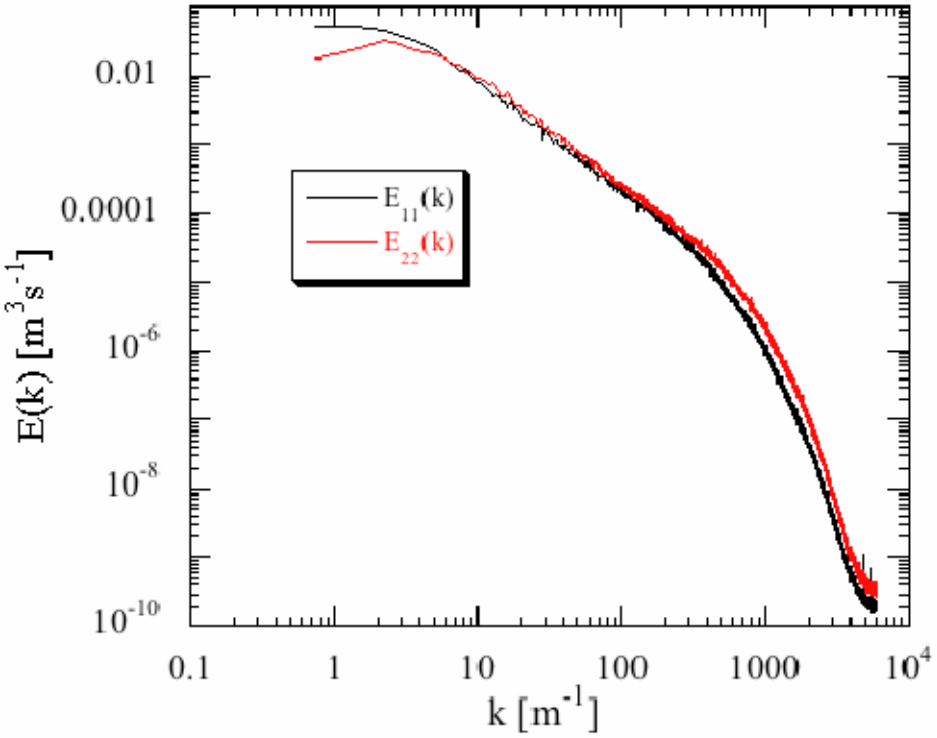

- Frame Rate = 8000 fps
- τ_η = 103 frames
- Tracking time = 0.125 sec = 10 τ_η

- ρ_{part} = 1000 kg/m^3 and ρ_{air} = 1.26 kg/m^3

Parameters:

- Parameters:
  - Reynolds number

$$R_\lambda = \frac{u\lambda}{\upsilon}$$

  - Stokes number

$$St \equiv \frac{\tau_p}{\tau_\eta} = \frac{\beta d^2 / 18\upsilon}{(\upsilon/\varepsilon)^{1/2}}, \quad \beta = \frac{\rho_p}{\rho}$$

  - Froude number

$$Fr_{inertial} = gSt \Big/ \left\langle a^2 \right\rangle^{1/2}$$

Movie of inertial particles (length of movie 8 τ_η)

- Frame rate of 8000 fps with resolution of 512 x 512 pixels.
- Laser at 40000 fps.
- Multiple shots per frame to increase visibility.
- Light sheet at 40 degrees, forward scatter.
- Sheet thickness about 2 mm.
- Projected area viewed 1.6 cm x 1.6 cm.

QuickTime™ and a
Cinepak decompressor
are needed to see this picture.

Tracks

- Mean speed 1.9 m/s
- R_λ ~ 250
- *St* ~ 0.09 and 0.15
- Kolmogorov length-scale 0.433 mm and time-scale 12.5 ms.
- Spatial resolution at least 37 μm (1/12th of η)
- Temporal resolution 0.125 ms (1/100th of τ_η)
- Integral scale 22 cm and integral time scale 1 sec
- Tracking distance 40 cm and tracking time approximately 0.2 sec

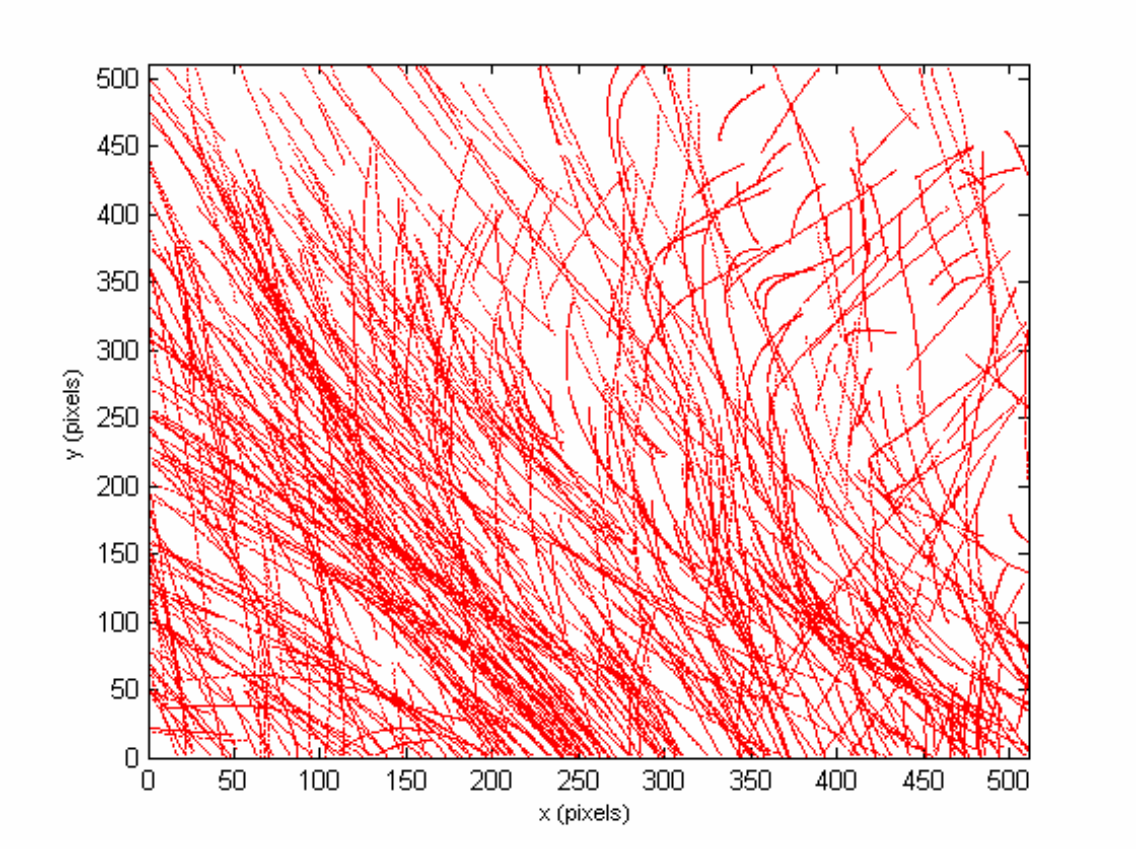

Sample Tracks

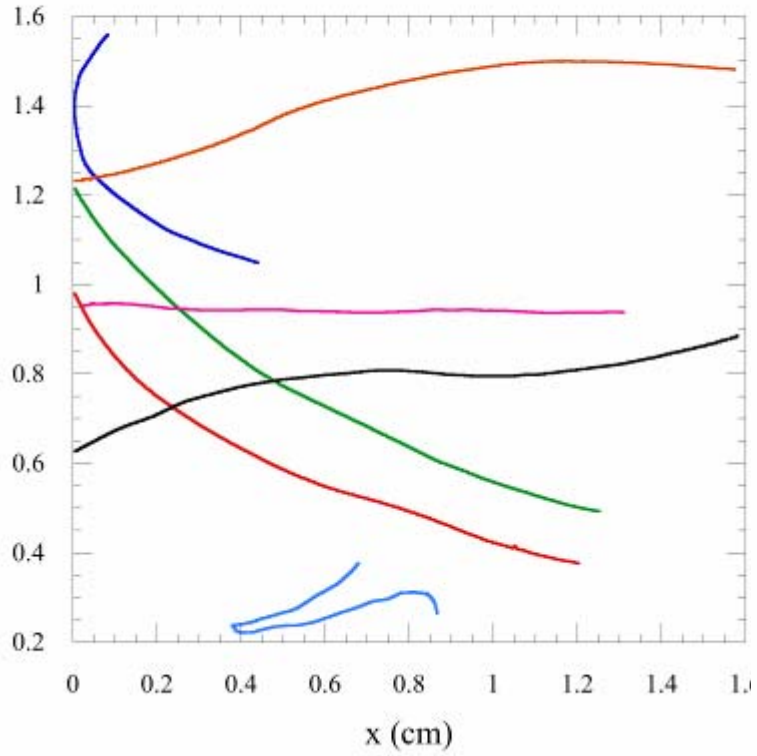

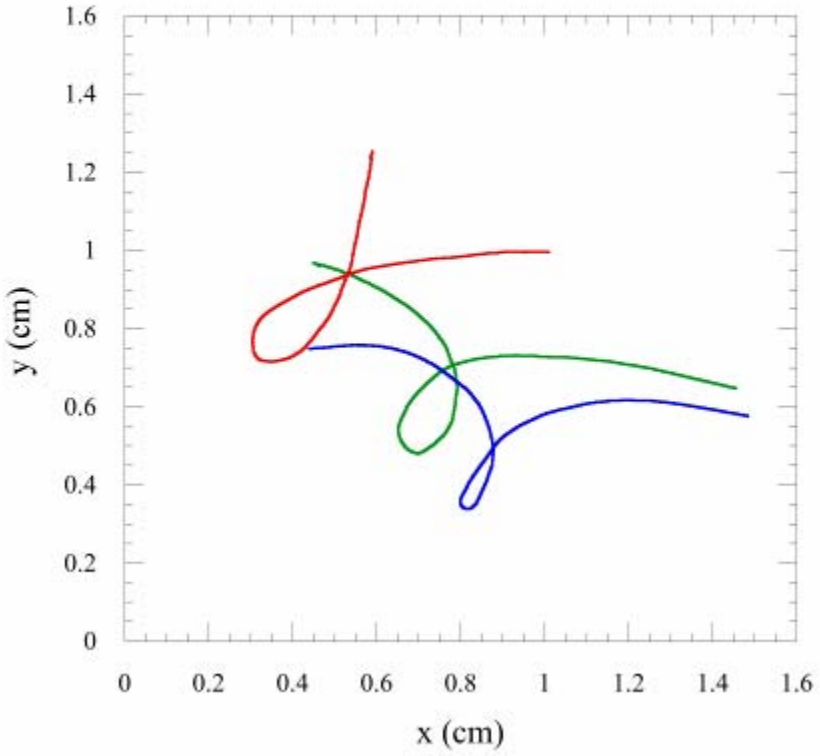

Particle size distribution

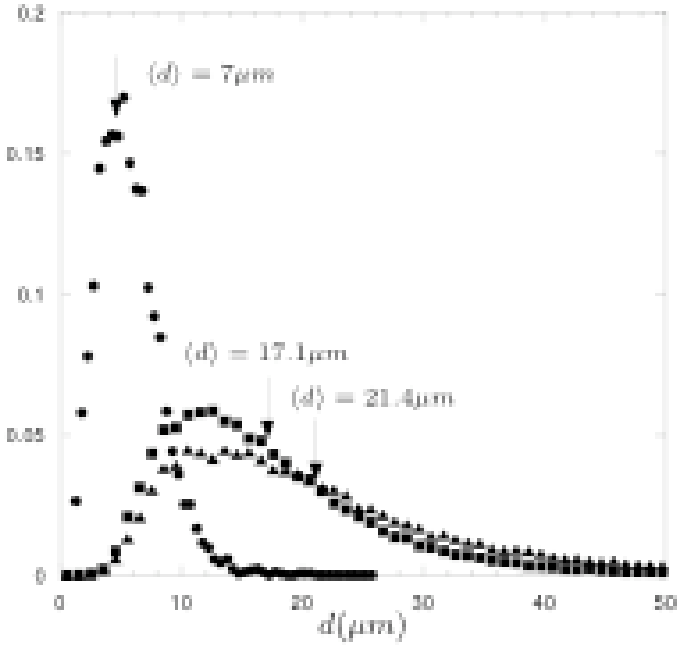

Fig. 2. . Particle size distributions at the measurement station. The vertical arrows are the mean diameters calculated from the distributions. The resulting mean Stokes numbers for the three cases are 0.01 ± 0.005 (circles), 0.09 ± 0.03 (squares) and 0.15 ± 0.04 (triangles).

Inertial Particle and Fluid Acceleration PDFs

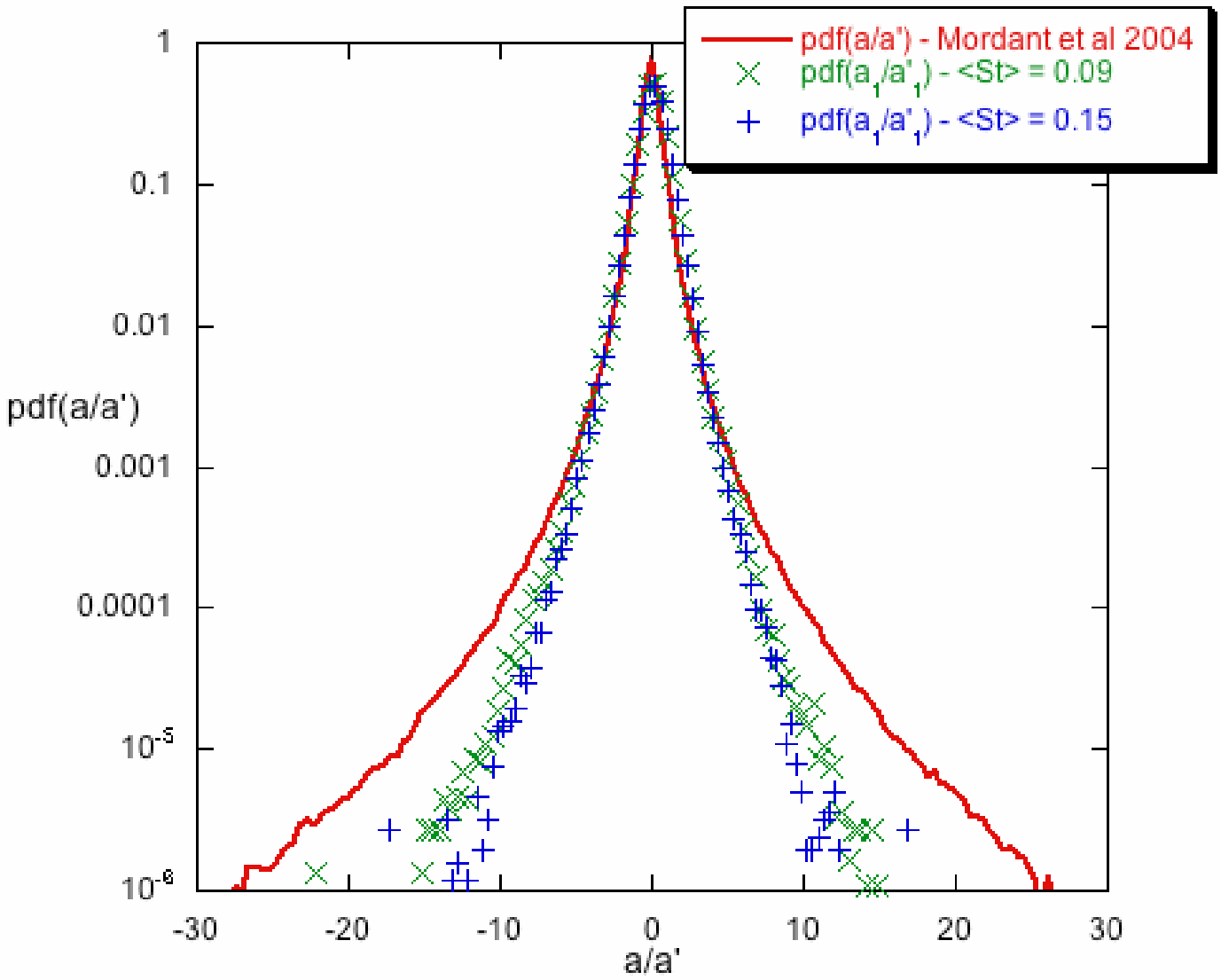

PRL Oct. 2000

Acceleration Probability density function

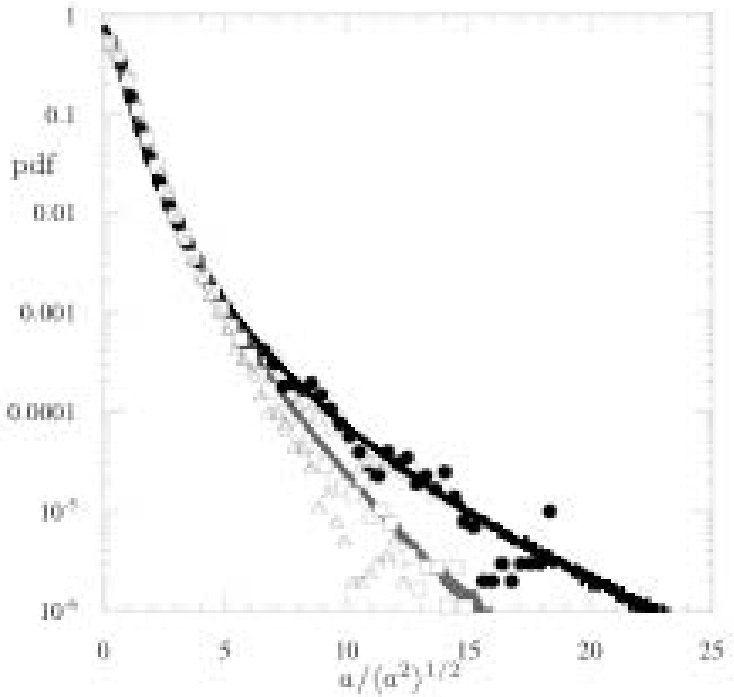

Fig. 4. The acceleration probability density functions (pdf). Inertial particles, squares $\langle St\rangle = 0.09 \pm 0.03$ and triangles, $\langle St\rangle = 0.15 \pm 0.04$ from Ayyalasomayajula et al. (2006) [2] and circles - passive particles ($\langle St\rangle = 0.01 \pm 0.005 << 1$, filled and open circles are pdfs for acceleration measured in x and y directions) at $R_\lambda = 250$. Also shown are the DNS results of comparable R_λ and St, from Bec et al. (2006) [3]: black line - fluid particles; gray line - $St = 0.16$ at $R_\lambda = 185$. The pdfs are of the acceleration normalized by the rms, $\langle a^2\rangle^{1/2}$.

Lagrangian Acceleration variance --- behavior with Reynolds number

$$\left\langle a_i a_j \right\rangle = a_0 \varepsilon^{3/2} \nu^{-1/2} \delta_{ij}$$

$$\left\langle a_i a_j \right\rangle \propto \left(L/\eta \right)^{3\mu/8} = R^{0.14}$$

$$\left\langle a_i a_j \right\rangle = a_0 \varepsilon^{3/2} \nu^{-1/2} \delta_{ij}$$

$$\left\langle a_i a_j \right\rangle \propto \left(L/\eta \right)^{3\mu/8} = R^{0.14}$$

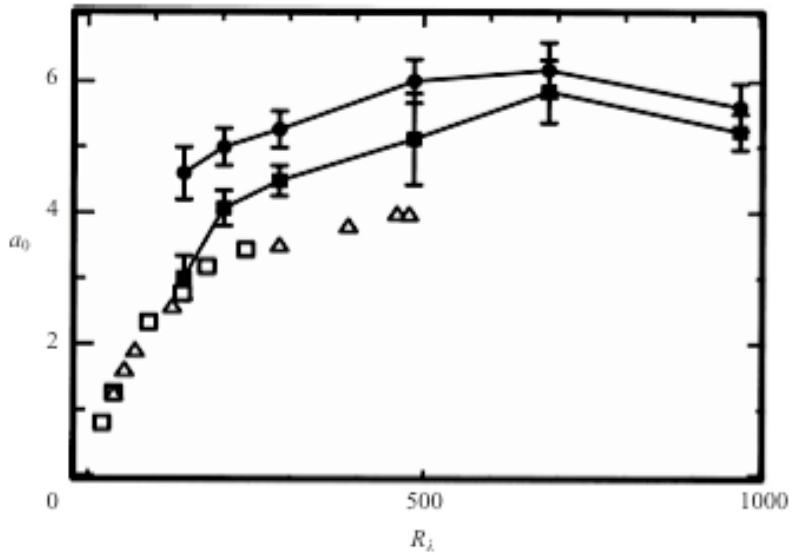

FIGURE 26. The Kolmogorov constant a_0 calculated for transverse (filled circles) and axial (filled squares) components of the acceleration, as a function of Reynolds number. These values have a 10% correction applied to them as discussed in §4.2. Values obtained from direct numerical simulation of turbulence by Vedula & Yeung (1999), and by Gotoh & Fukayama (2001) are also shown by open squares and open triangles, respectively.

Acceleration variance vs Reynolds number

Inertial Particles--Preferential Concentration

(Evenly distributed inertial particles concentrate in regions of high strain)

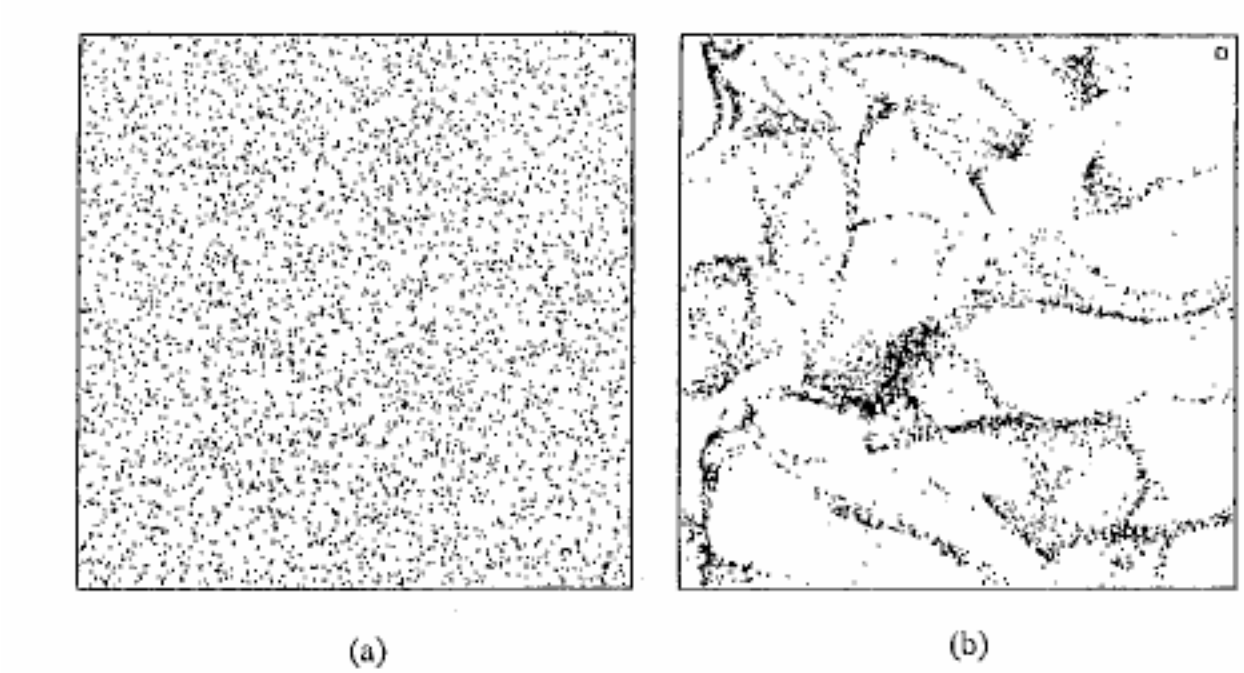

From Shaw, Reade, Collins and Verliade J.A.S ,55,1998

Radial distribution

$$\eta(r) = \frac{\langle \rho_p(r) \rangle}{\rho_p} - 1$$

where $\langle \rho_p(r) \rangle$ *is the particle density at a distance r relative to each particle averaged over all particles and* ρ_p *is the global particle density*

$$\eta(r) \propto (r/r_k)^{-f(St)}$$

$$St = \frac{\tau_d}{\tau_k} = \frac{1}{18}\left(\frac{\rho_d}{\rho}\right)\left(\frac{d}{r_k}\right)^2$$

Shaw et al. Radial Distribution Measurements in Cornell tunnel with active grid

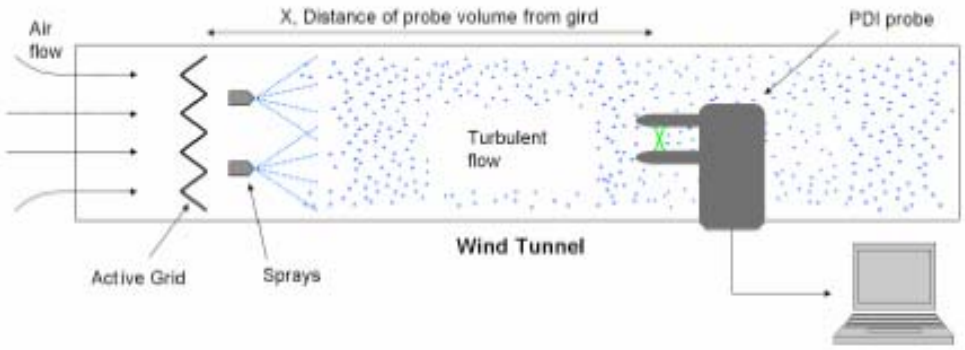

FIG. 1: Experimental setup, including wind tunnel with active grid, spray nozzles, and the phase Doppler interferometer for measuring droplet arrival time, size, and longitudinal speed.

Experiment	3m20Hz	3m30Hz	5m20Hz	5m30Hz
R_λ	520	660	440	590
$\varepsilon\ (m^2 s^{-3})$	1.6	5.4	0.6	2.0
U (ms^{-1})	4.69	6.78	4.59	6.81
u/U	0.17	0.18	0.12	0.13
$r_k\ (\mu m)$	210	150	270	200

Radial Distribution Function. R Shaw et al

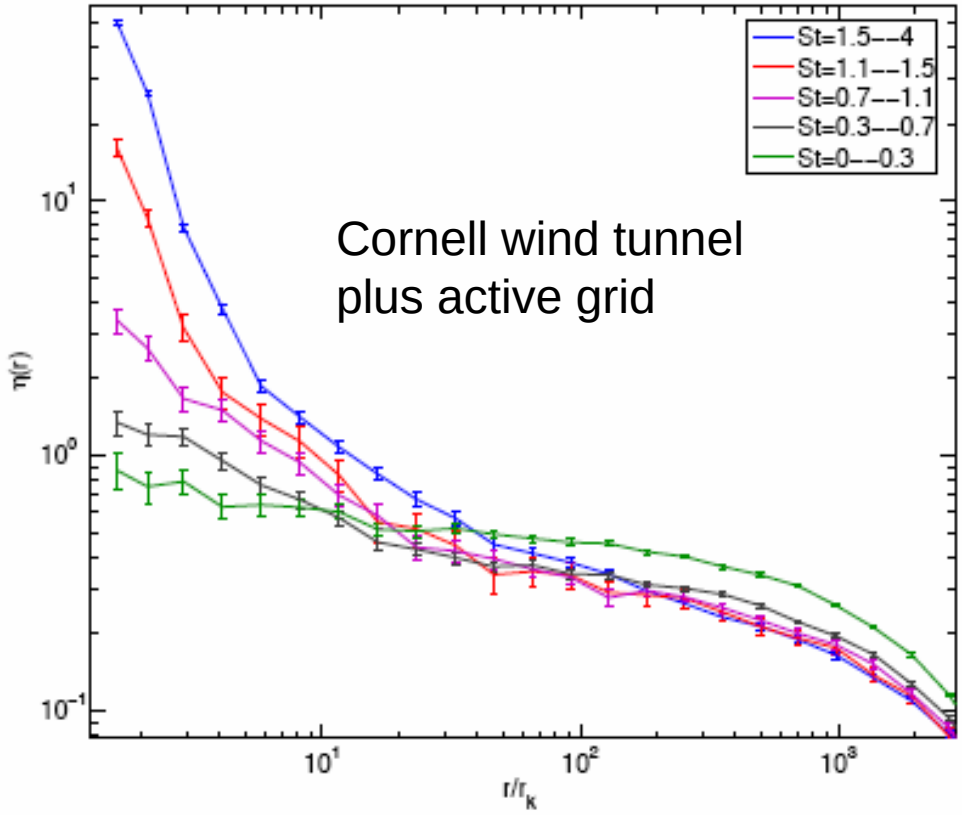

FIG. 2: (color online) $\eta(r)$ versus $\hat{r}$ ($\equiv r/r_k$) with error bars of 2σ, and with $\eta(r)$ parameterized by St from experiment 3m30Hz. Each line is $\eta(r)$ calculated from droplets within a particular St range, specified in the legend, with the order from bottom to top corresponding to successively larger St.

Stokes Number Similarity: St = 0.001- 0.3 (circles) and St = 0.7- 1.1(triangles)

(Reynolds number is varied)

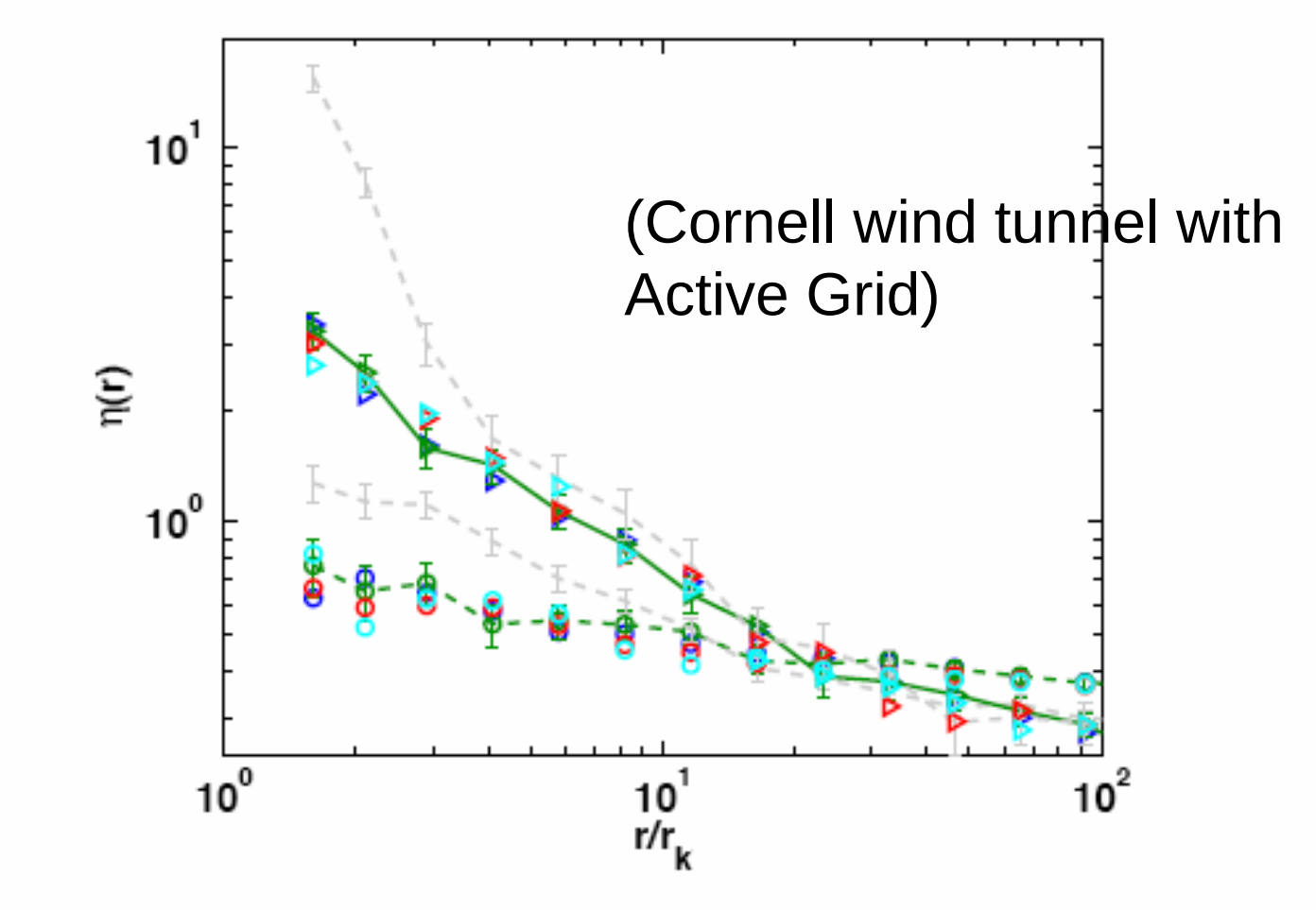

R A Shaw et al 2006

MIXING

For mixing need to know separation rate of pairs of fluid elements:
Classical Richardson-Obukhov:
Mean square separation proportional to t^3
Batchelor considers initial separation:

$$\left\langle \left[\vec{\Delta}(t) - \vec{\Delta}_0 \right]^2 \right\rangle = \frac{11}{3} C_2 (\varepsilon \Delta_0)^{2/3} t^2 \; for \; t < t_0 = \left(\frac{\vec{\Delta}_0^2}{\varepsilon} \right)^{1/3}$$

(Turbulence is super-diffusive--Brownian~t)

Lagrangian measurements. Bourgoin et al Science,311

835,2006

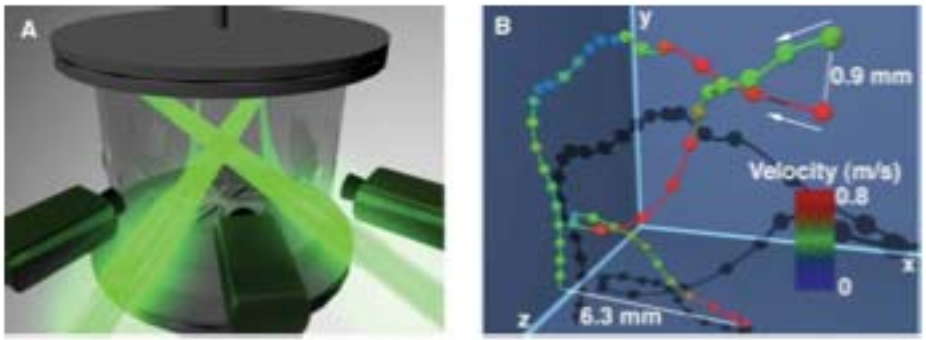

Fig. 1. (**A**) Sketch of the experimental setup. Three high-speed cameras were used to record the three-dimensional tracks of tracer particles in intense turbulence. The particles were illuminated by two high-power lasers. (**B**) A pair of measured particle trajectories at $R_\lambda = 690$. The small spheres mark every other measured position of the particles and are separated by 0.074 ms ($=\tau_\eta/13$) in time; the large spheres mark every 30th position. The color of the spheres indicates the magnitude of each particle's absolute velocity in units of m/s. The particles enter the measurement volume as indicated by the arrows and separate under the influence of the turbulence.

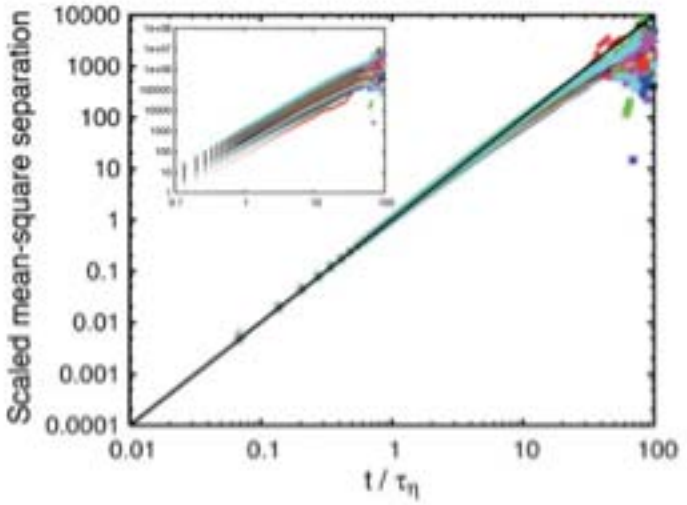

Fig. 2. Evolution of the mean square particle separation. The mean square separation between particle pairs is plotted against time for 50 different initial separations at a turbulence level of $R_\lambda = 815$, with the time axis normalized by the Kolmogorov scales. Each curve represents a bin of initial separations 1 mm wide ($=43\eta$), ranging from 0 to 1 mm to 49 to 50 mm. The curves are scaled by the constant $(\frac{11}{3})C_2(\varepsilon\Delta_0)^{2/3}$ (Eq. 1). The data collapse onto a single universal power law. The bold black line is the power law predicted by Batchelor (*11*). Because the smallest Δ_0 measured is not in the inertial range, we do not expect it to scale perfectly as t^2, and indeed it does not scale as well as the larger Δ_0. The inset shows the same curves scaled simply by the Kolmogorov length, for which we see no scale collapse. For both plots, we see no Richardson-Obukhov t^3 scaling.

Eulerian line sources in Grid Turbulence

Warhaft JFM 1984

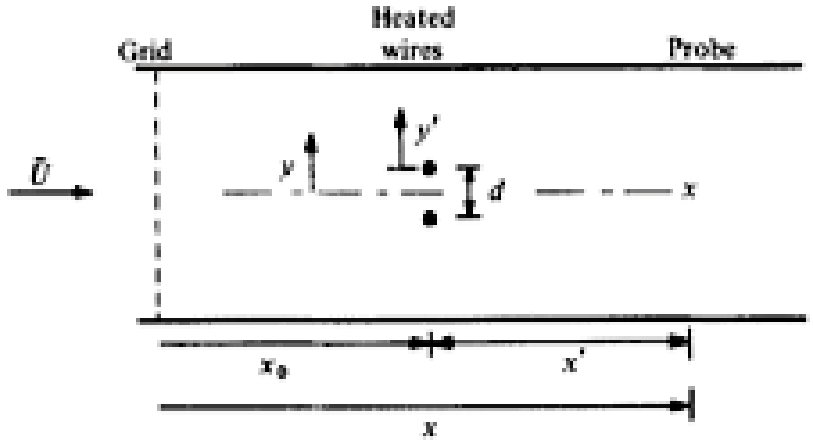

FIGURE 1. Sketch of wind tunnel showing two heated wires. When two or more heated wires are used the transverse direction y (through which the probe is moved) is measured from the midpoint between the two central wires. For experiments with one wire only (figures 4 to 12) the transverse direction y' is measured from the wire itself.

Line sources continued

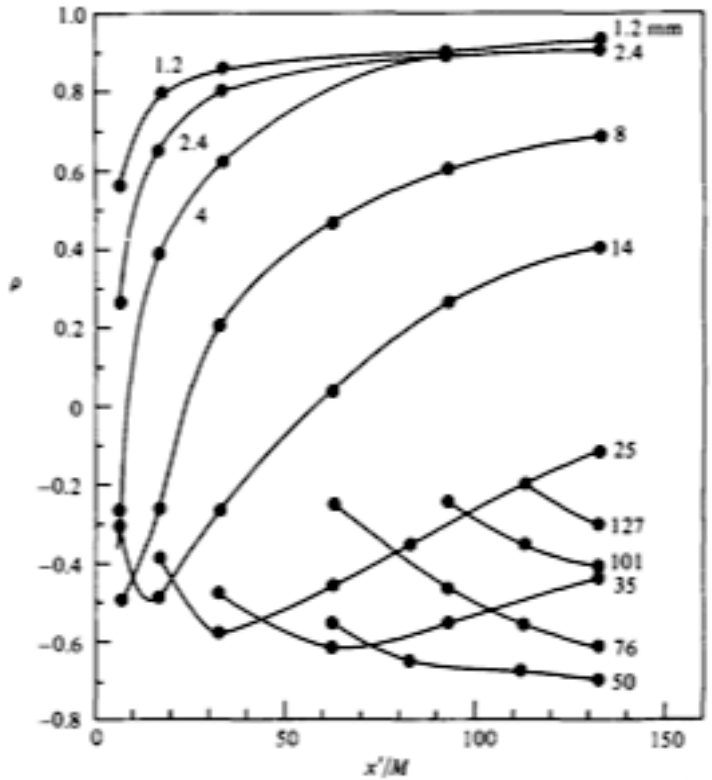

FIGURE 14. ρ versus x'/M for experiments such as shown in figure 13. ρ is for the midpoint between the wires (y = 0, figure 1). The numbers are the wire spacing d (mm). The wires are at $x_0/M = 20$.

Line sources continued.

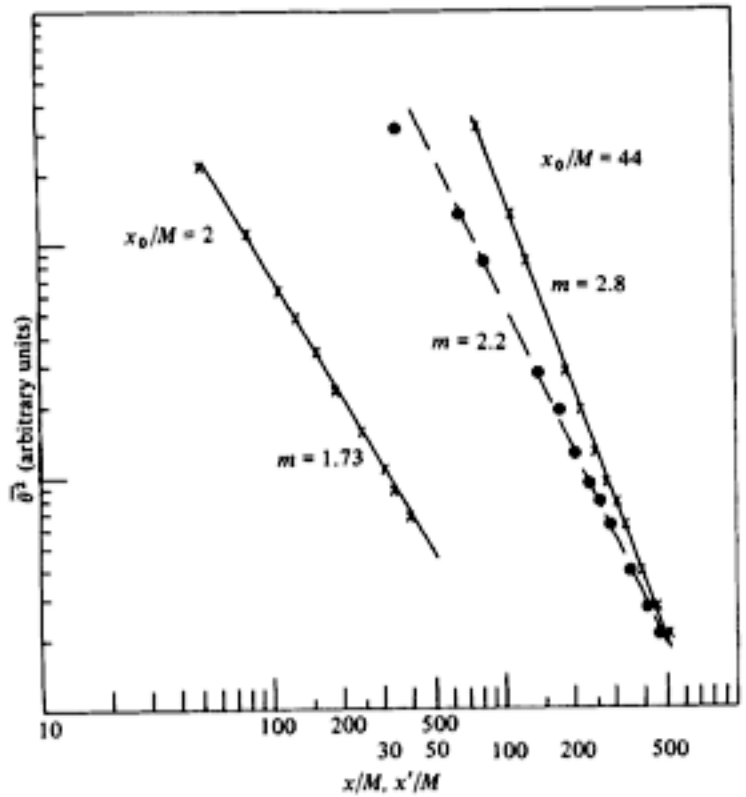

FIGURE 21. The decay of temperature variance for a mandoline of 1.69 cm wire spacing placed at $x_0/M = 2$ (left-hand graph) and $x_0/M = 44$ (right-hand graph) from the grid. $M = 0.84$ cm. Crosses, $\overline{\theta^2}$ versus x/M; dots, $\overline{\theta^2}$ versus x'/M.

Strong dependence on initial conditions in both Eulerian and Lagrangian frameworks

Bodenschatz ” washing machine “

Anisotropy measurements

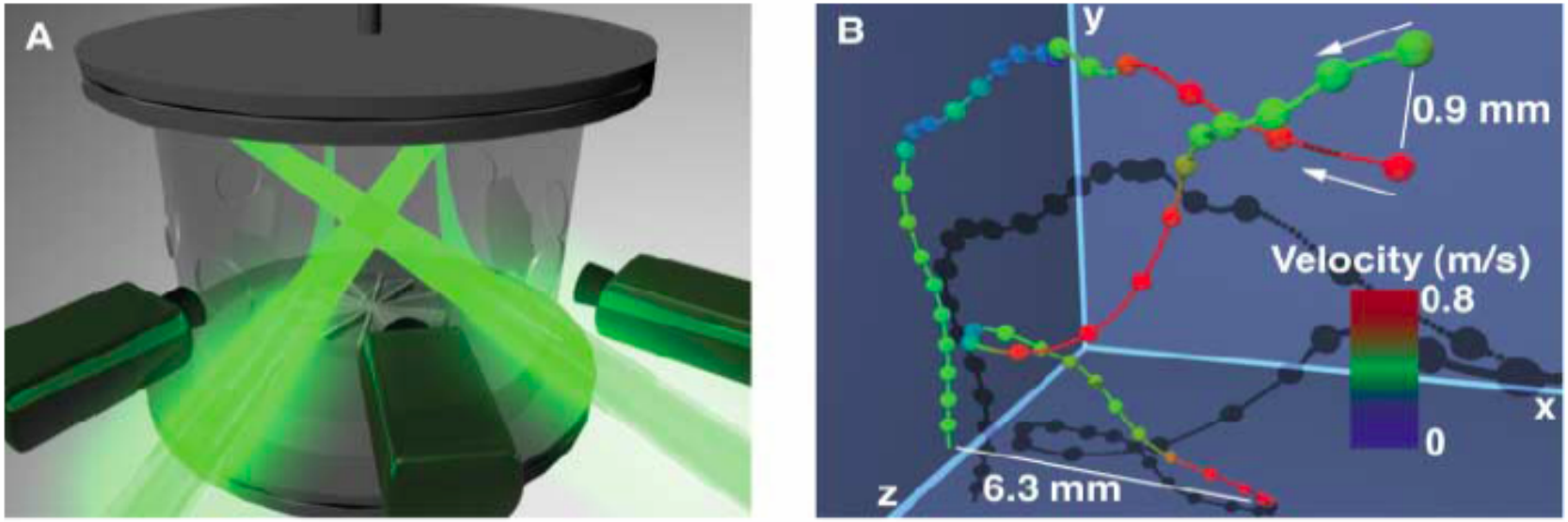

Fig. 1. (**A**) Sketch of the experimental setup. Three high-speed cameras were used to record the three-dimensional tracks of tracer particles in intense turbulence. The particles were illuminated by two high-power lasers. (**B**) A pair of measured particle trajectories at $R_\lambda = 690$. The small spheres mark every other measured position of the particles and are separated by 0.074 ms ($\approx\tau_\eta/13$) in time; the large spheres mark every 30th position. The color of the spheres indicates the magnitude of each particle's absolute velocity in units of m/s. The particles enter the measurement volume as indicated by the arrows and separate under the influence of the turbulence.

zz is axial , yy and xx are radial

Measurements of Lagrangian statistics of fluid particles at high Reynolds number

$$\delta u_i(\tau) = u_i(t+\tau) - u_i(t)$$

Lagrangian Structure Function:

$$D_{ij}^{L}(\tau) = \left\langle \delta u_i(\tau) \delta u_j(\tau) \right\rangle = C_0 \varepsilon \tau \delta_{ij}$$

C_0 *should be universal and* D_{ij}^{L} *should be isotropic*

Ouellette et al NJP 8 (2006),102.
Lagrangian Structure functions.

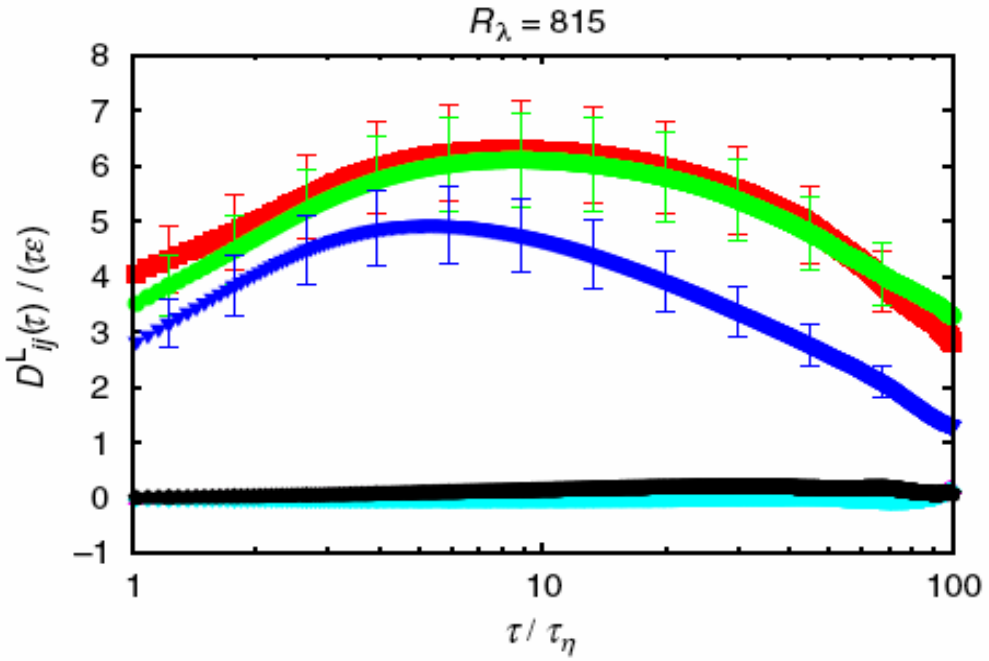

Figure 4. The xx (■), yy (●) and zz (▼) components of the compensated Lagrangian structure function at $R_\lambda = 815$. The other symbols show the off-diagonal components. The time axis has been normalized by the Kolmogorov time. The relative magnitude of the radial and axial components reflects the anisotropy of our large-scale flow.

Anisotropy ratio - Lagrangian

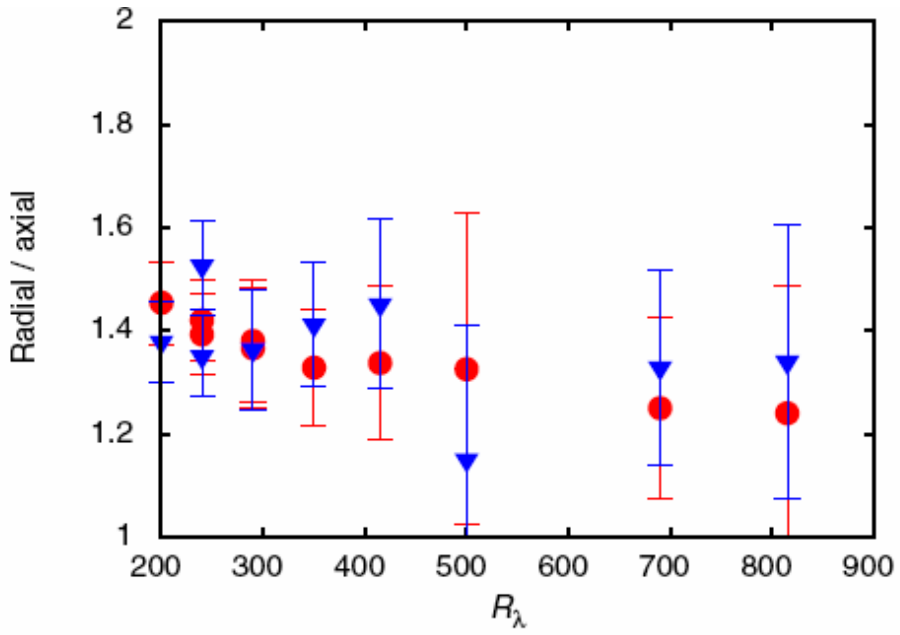

Note : the Lagrangian structure function scaling exponents Saturate (H. Xu et al PRL ,2006).
As for passive scalar.

Figure 8. The ratio of the radial to the axial measurements of C_0 as a function of Reynolds number from both the structure function (●) and the spectrum (▼). While the anisotropy decreases weakly with increasing Reynolds number, the measurements remain far from isotropic even at the highest Reynolds numbers measured.

C_0 from Lagrangian Structure Functions. Ouellette et al (2006)

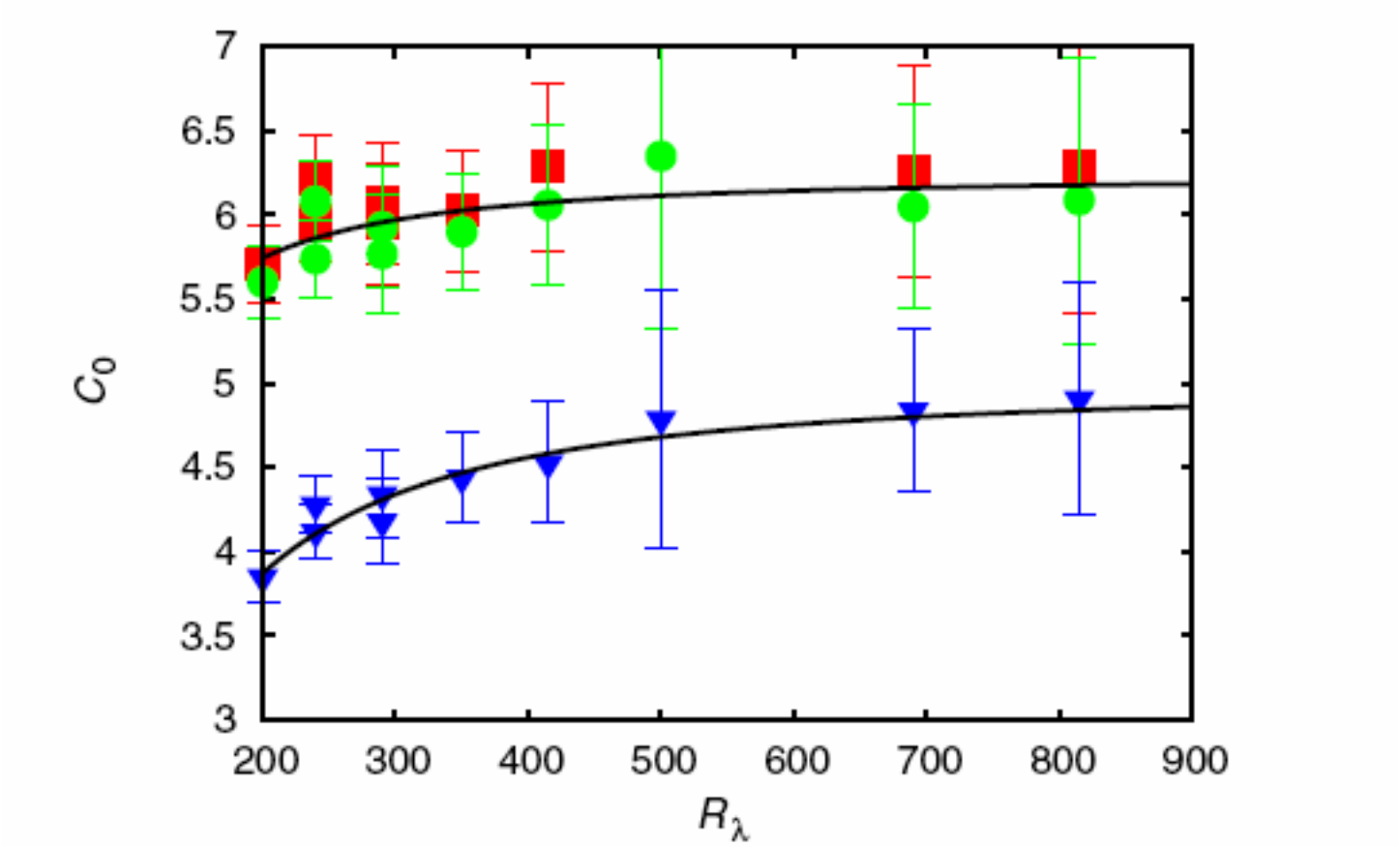

Homogeneous Shear Experiments

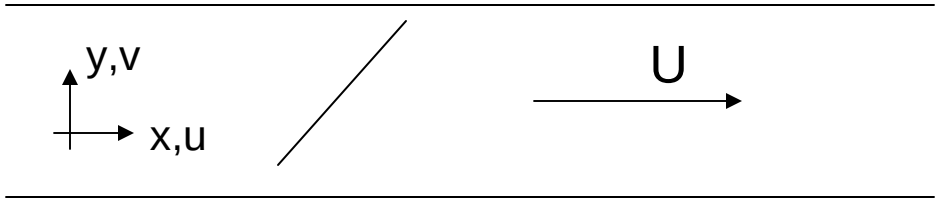

For isotropy, skewness should tend to zero at high Re

$$S_{\partial u/\partial y} \equiv \frac{\left\langle (\partial u/\partial y)^3 \right\rangle}{\left\langle (\partial u/\partial y)^2 \right\rangle^{3/2}}$$

What about 5th and 7th moments.
Here, separating the effects of intermittency we define,

$$H_{\partial u/\partial y} \equiv \frac{\left\langle (\partial u/\partial y)^5 \right\rangle}{\left\langle (\partial u/\partial y)^4 \right\rangle^{5/4}} \qquad SH_{\partial u/\partial y} \equiv \frac{\left\langle (\partial u/\partial y)^7 \right\rangle}{\left\langle (\partial u/\partial y)^6 \right\rangle^{7/6}}$$

How do they vary with Re?

Schumacher et al

Phys. Fluids, Vol. 15, No. 1, January 2003

Schumacher, Sreenivasan, and Yeung

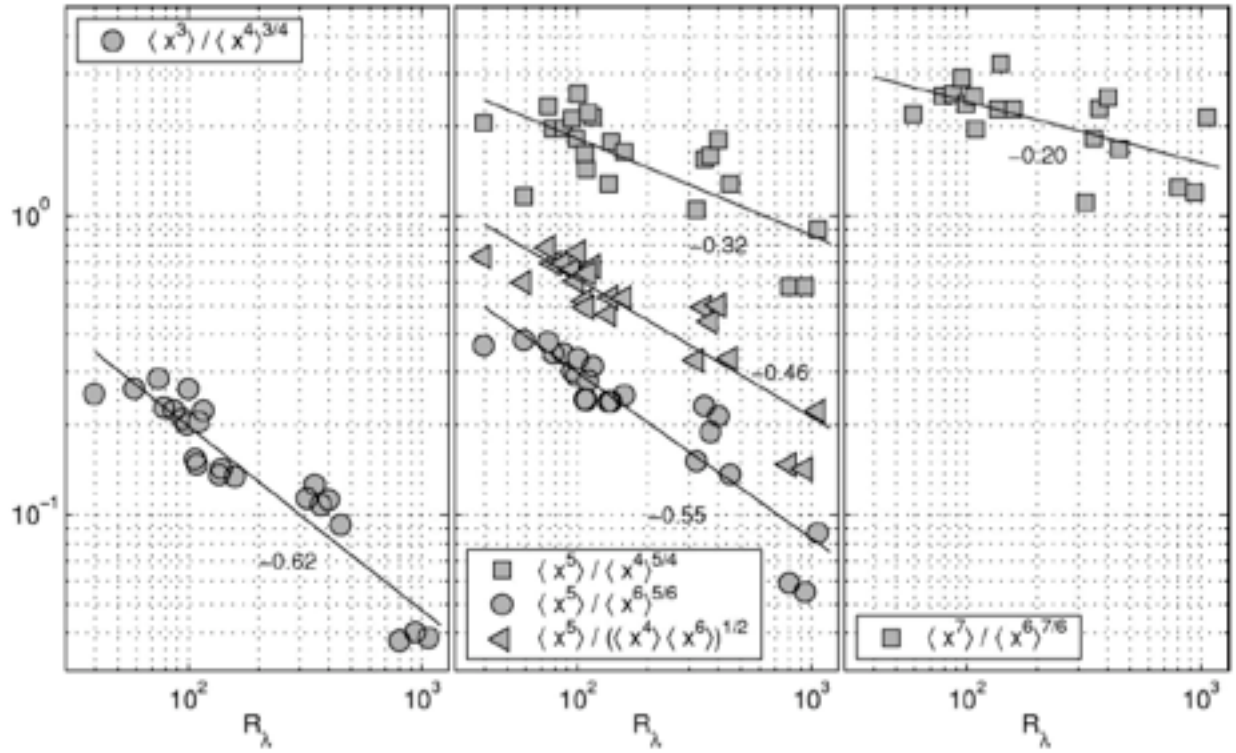

Normalized 3rd, 5th and 7th transverse derivative moments.

(How do we normalize the 4th and 6th order Structure Functions?
See Warhaft anf Gylfasson, Advances in Turbulence , X)

A new high Re tunnel

Taylor Reynolds number ~ 10,000

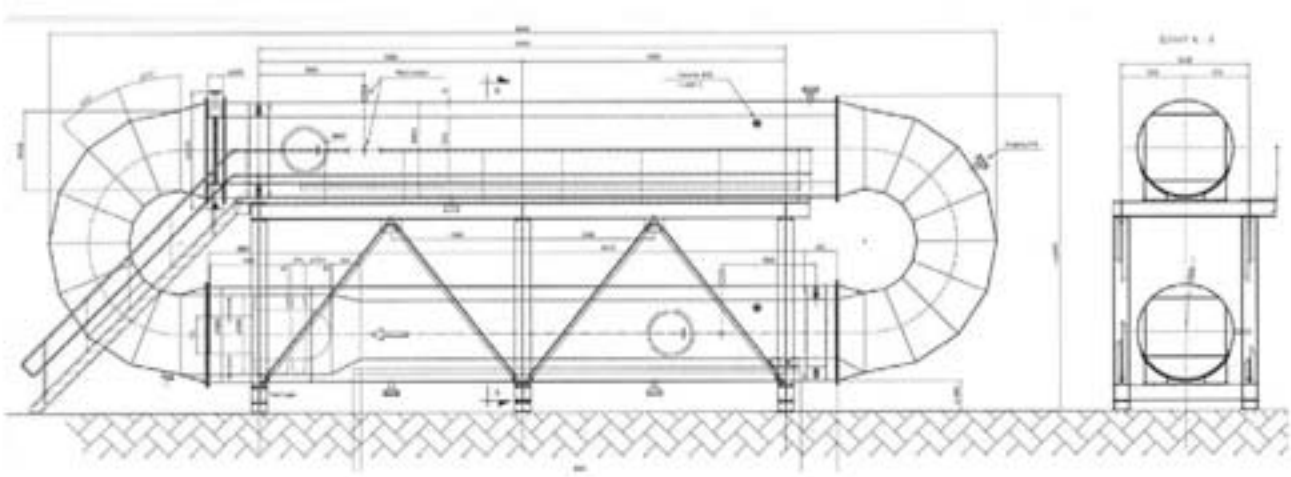

Figure 1: Schematic of the high-Reynolds-number wind tunnel under construction at the Max Planck Institute for Dynamics and Self-Organization (MPIDS) in Goettingen under the direction of Prof. Eberhard Bodenschatz.

Environment vs. Laboratory studies

Atmospheric measurements were first to tell us about :

-sharp fronts (ramp-cliffs), scalar anisotropy, Kolmogorov scaling…….

Observations were refined by experiments and computations

Laboratory measurements have yielded structures, new statistics (pdf's, radial distributions etc) and details on small scale structure, reactions and mixing.

The atmosphere and oceans will remain the ultimate high Re lab but its non stationarity and lack of repeatability necessitate lab experiments.

FIN

Eulerian structure function exponents

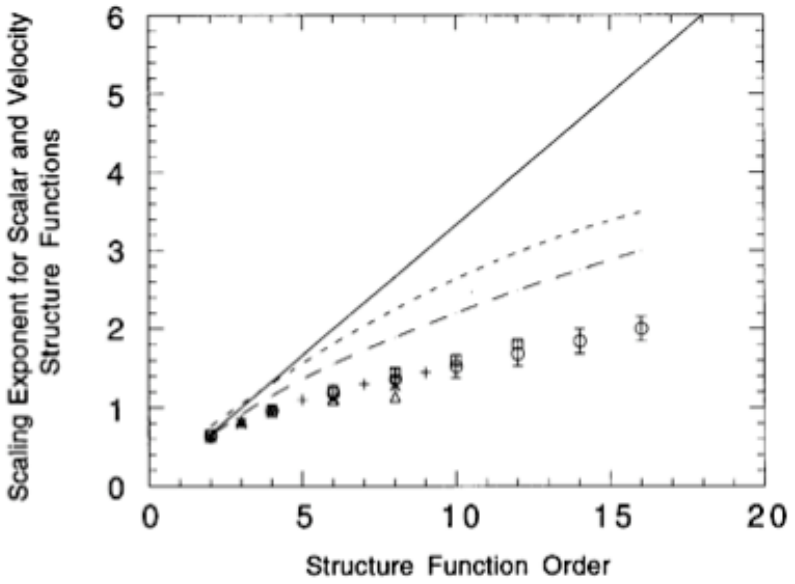

Figure 11 The scaling exponent ζ_n for the scalar structure function $\langle[\Delta\theta(r)]^n\rangle$ within the inertial subrange as a function of n. *Squares* are from the data of Antonia et al (1984) (heated jet), *crosses* are from the data of Ruiz-Chavarvia et al (1996) (heated wake), *triangles* are from the data of Meneveau et al (1990) (heated wake), *circles* are from the data of Mydlarski & Warhaft (1998a) (grid turbulence), and *plus signs* are from the full, three dimensional Navier-Stokes numerical simulations of Chen & Kraichnan (1998). *Vertical bars* represent uncertainty for the Mydlarski & Warhaft data. The *long-dashed line* is the white-noise estimate from Kraichnan (1994). *The short-dashed line* is for the velocity field from Anselmet (1984). The solid line is the KOC prediction.

High Reynolds Number Axi-symmetric strain

Experimental Setup

$$40 \geq R_\lambda \leq 47($$

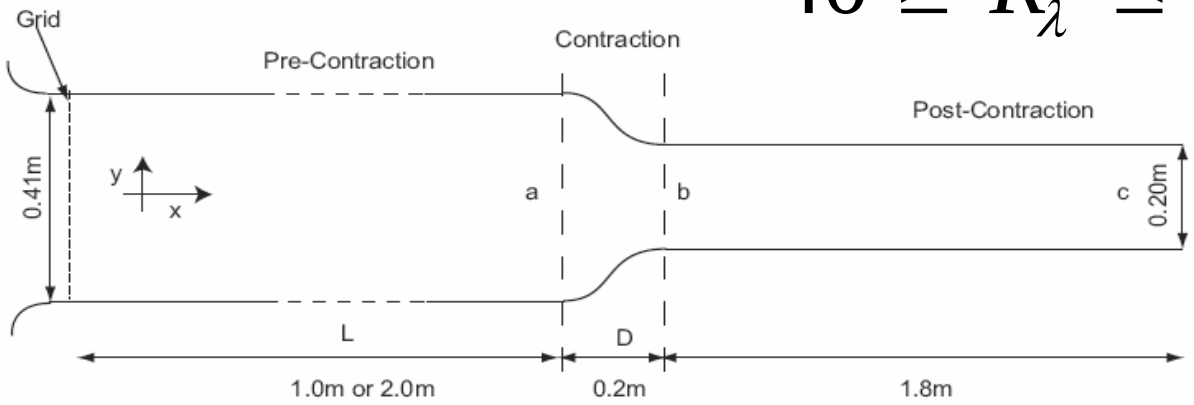

Schematic of the experimental setup. Two different pre–contraction sections were used. Active and passive grids were used to vary the Reynolds numbers. a and b are the immediate pre– and post–contraction regions respectively. c is the furthest downstream distance location, 153 cm from the end of the contraction.

S Ayyalasomayajula and Z W

Relaxation of strained spectra towards isotropy

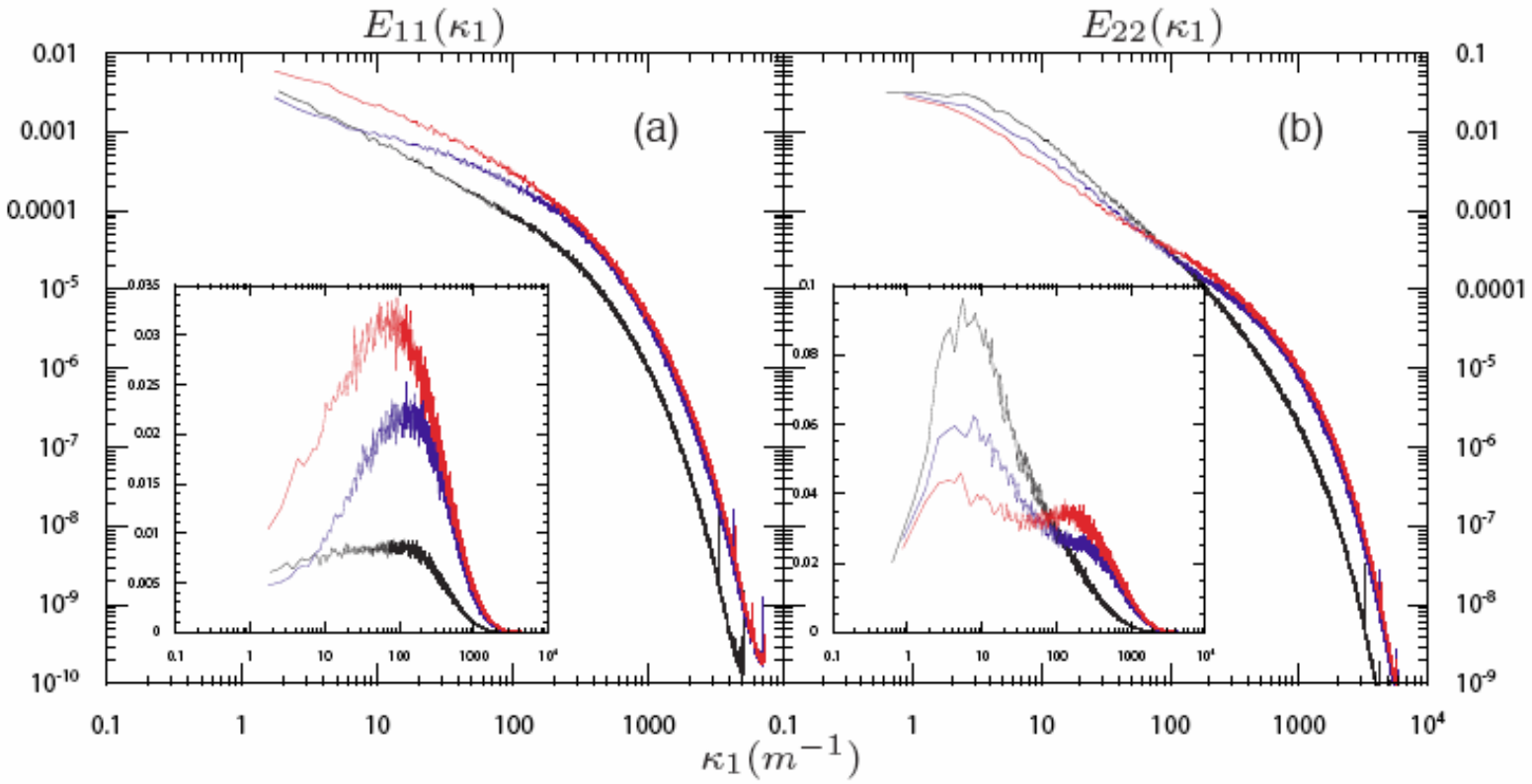

One dimensional Energy spectra, downstream evolution; RL, Re_{λ_a} = 260, S^* = 24: (a) $E_{11}(\kappa_1)$, inset $\kappa_1 E_{11}(\kappa_1)$;(b) $E_{22}(\kappa_1)$, inset $\kappa_1 E_{22}(\kappa_1)$; — station b; — intermediate station; — station c.

Complex spectral dynamics

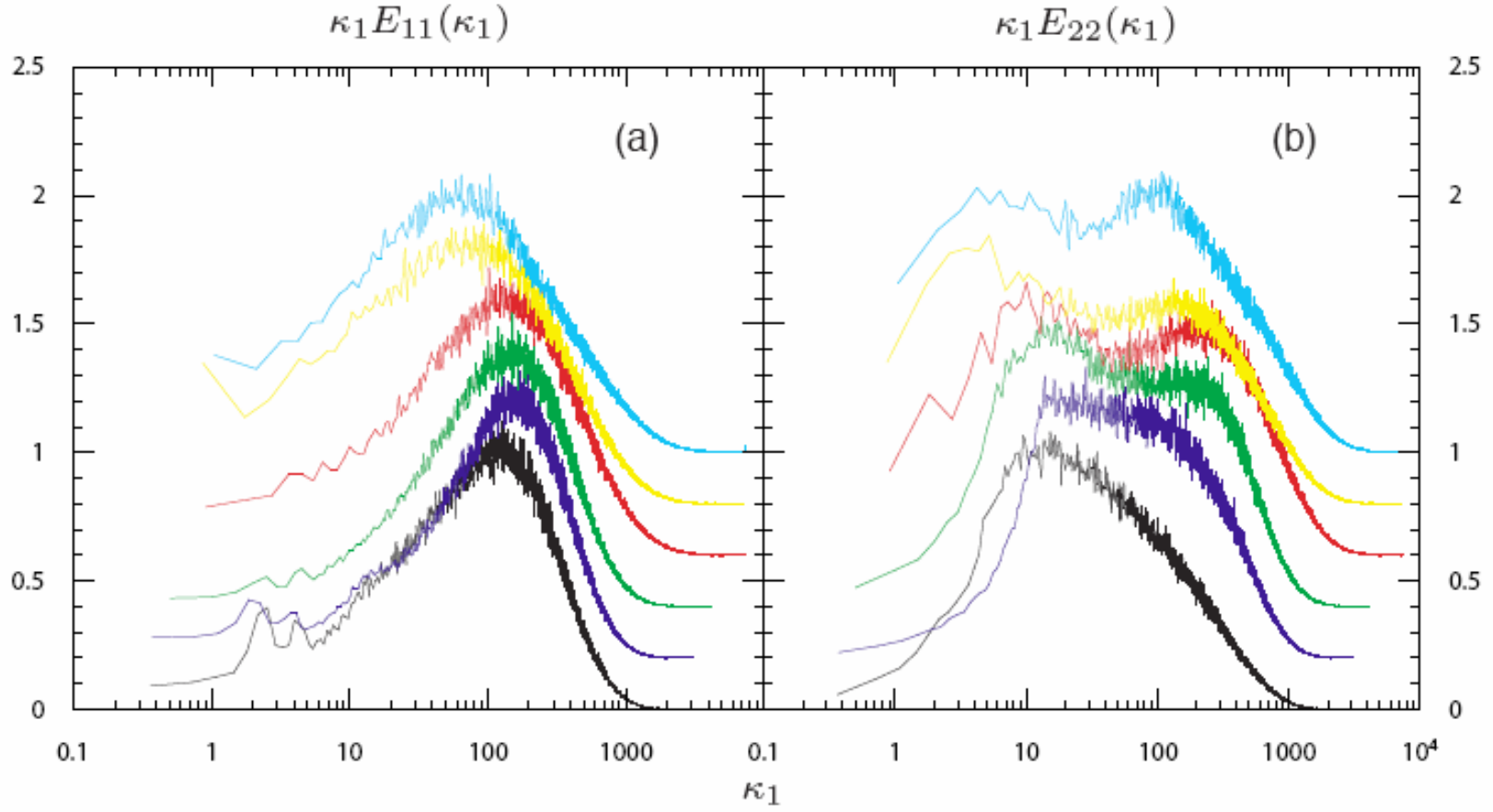

Normalized one dimensional Energy spectra, final evolved spectra: — 2PL, $R_{\lambda_a} = 52$, $S^* = 32$; — 1PS, $R_{\lambda_a} = 44$, $S^* = 12$; — 2PS, $R_{\lambda_a} = 64$, $S^* = 12$; — SS, $R_{\lambda_a} = 170$, $S^* = 12.5$; — RL, $R_{\lambda_a} = 260$, $S^* = 24$; — RS, $R_{\lambda_a} = 470$, $S^* = 17$.

A Closer Look at the PDFs

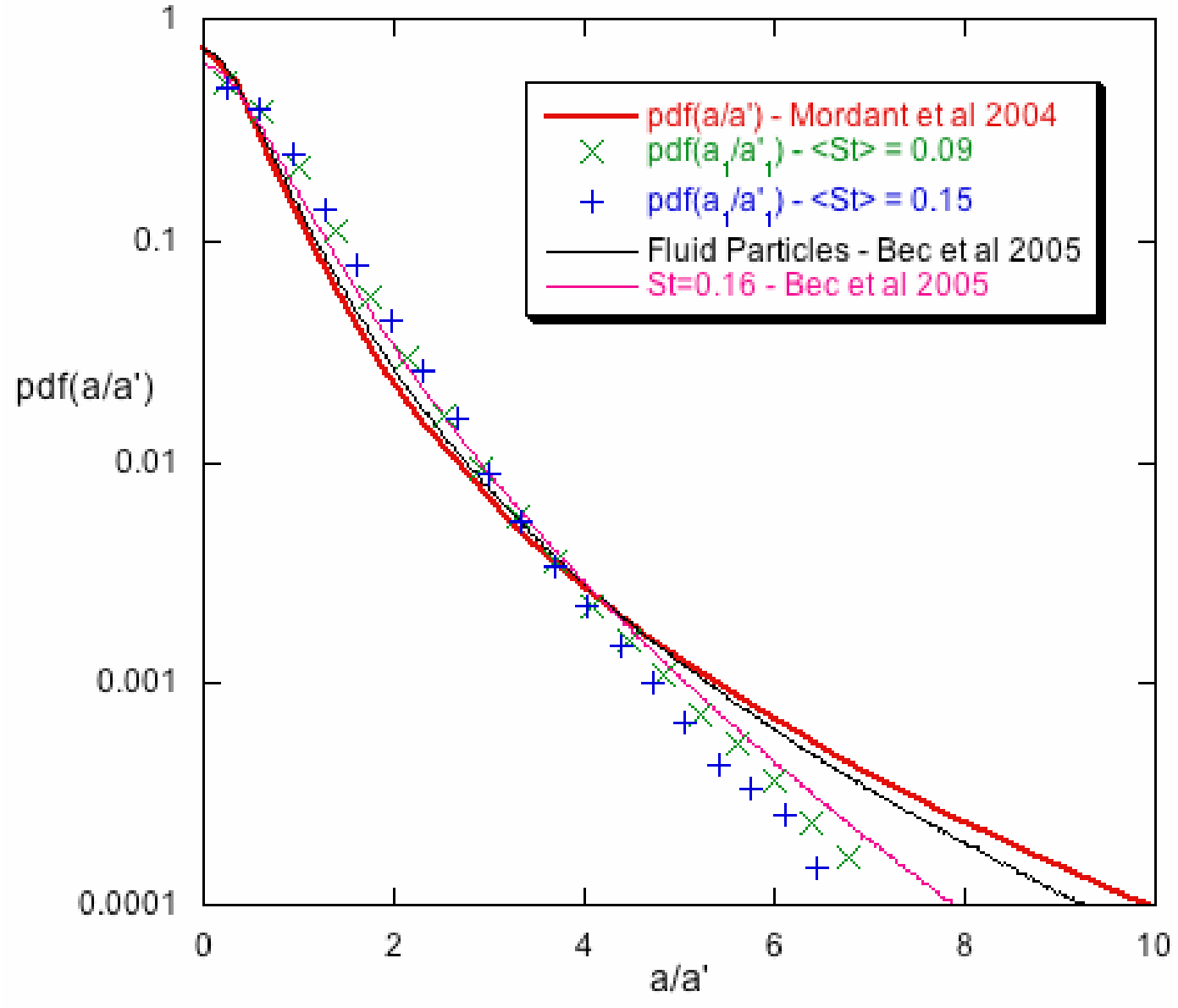

Comparison with DNS

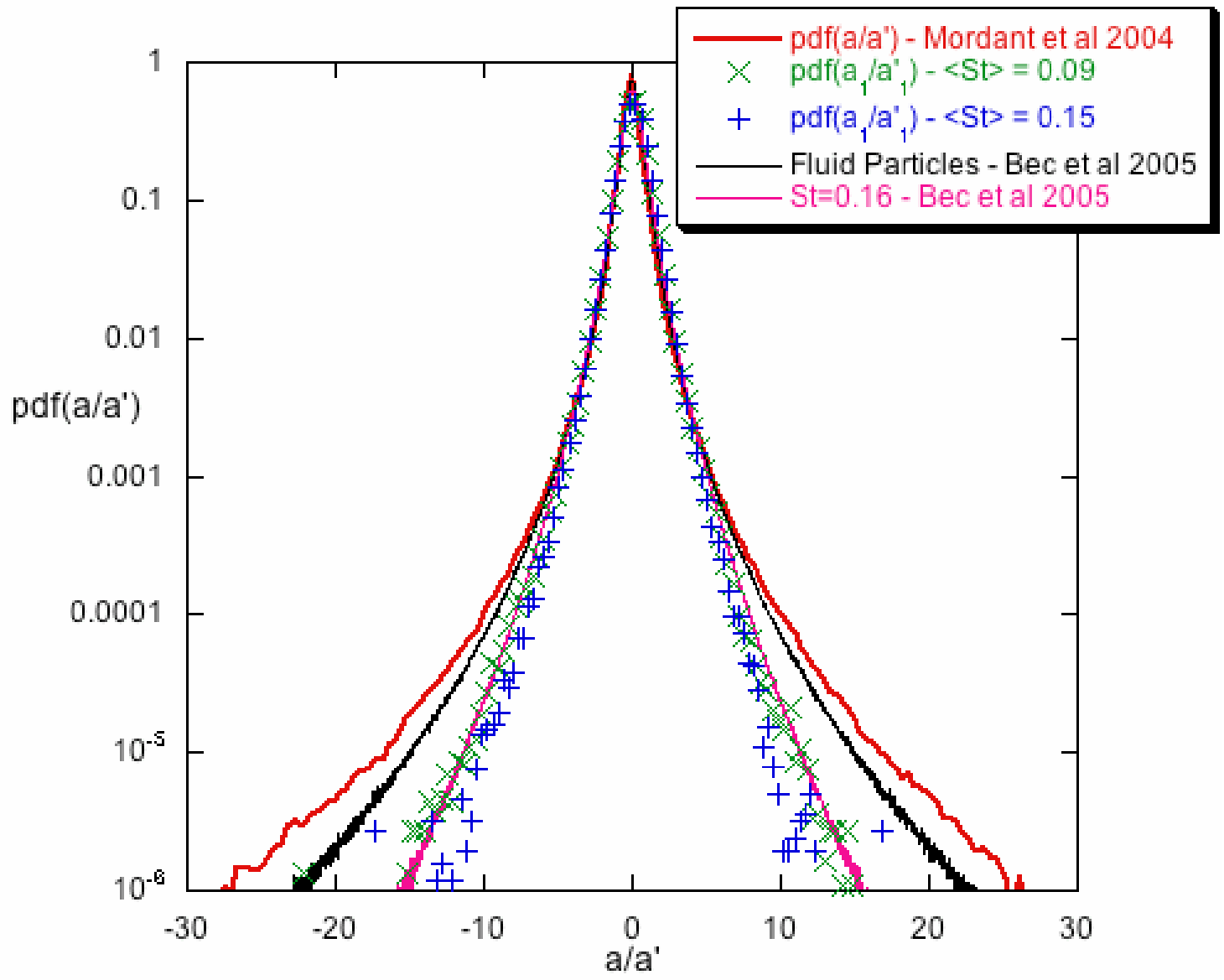

Spray Characteristics

- Spray injected directly behind turbulence generating grids.
- Spray injected approximately at mean velocity of the flow.
- Mass loading can be varied between 10^{-4} - 10^{-3} (kg of water / kg of air)
- Number density 30 - 300 per cc for 20μm water droplets
- Particle size distribution log-normal.
- Distribution can be varied by changing atomizing air and water pressures.

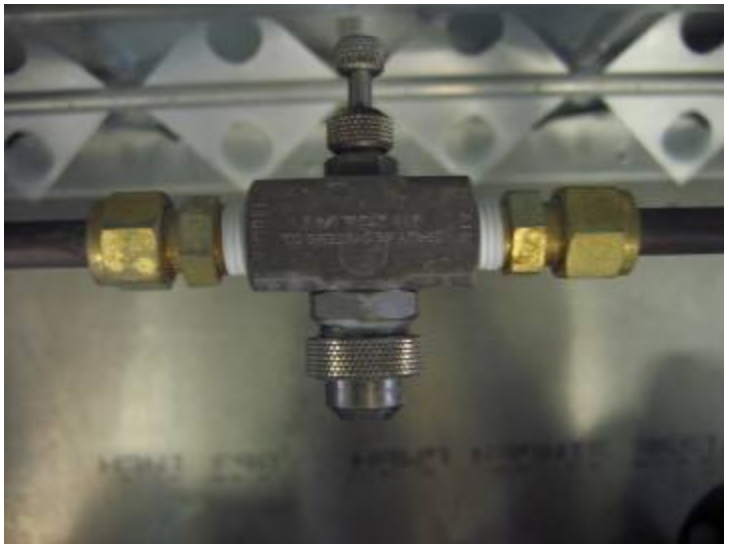

Spray System

- 4 air atomizing nozzles generate narrow distribution water droplets.
- Closed loop electro-pneumatic valves maintain accurate atomizing pressures.

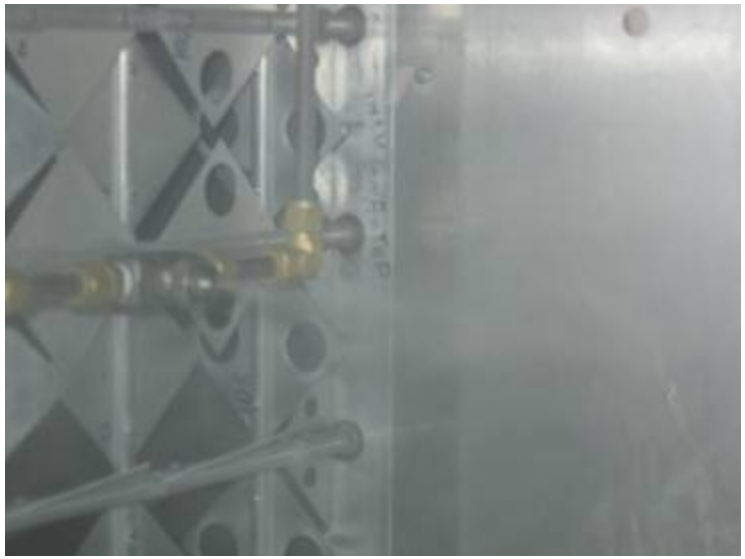

•Spray injected directly behind turbulence generating grids.

•Spray injected approximately at mean velocity of the flow.

•Mass loading can be varied between 10^{-4} - 10^{-3} (kg of water / kg of air)

•Number density 30 - 300 per cc for 20μm water droplets

•Particle size distribution log-normal.

•Distribution can be varied by changing atomizing air and water pressures

Conclusions

- There is significant progress in Lagrangian turbulence experiments.(Lyon, RISO,ETH,Marburg,Max-Planck,Cornell…..).
- We look forward to new results on passive as well as inertial fluid particles . High Re and high Stokes numbers…..
- Lagrangian experiments pose significant new problems: High Re asymptotes appear to be higher than for the Eulerian.Need for “super “ high Re with all its technical challenges